Biointerface Research in Applied Chemistry
Open-Access Journal (ISSN: 2069-5837)

Article
Volume 13, Issue 1, 2023, 76
https://doi.org/10.33263/BRIAC131.076

Identification of Novel Indole Derivatives as Potent α-Amylase Inhibitors for the Treatment of Type-II Diabetes Using in-Silico Approaches

Khalil El Khatabi [1,*], Reda El-Mernissi [1], Halima Hajji [1] Atul Kumar Singh [2], Mohammed Aziz Ajana [1], Tahar Lakhlifi [1], Shashank Kumar [2,*], Mohammed Bouachrine [1,3]

[1] Molecular chemistry and Natural Substances Laboratory, Faculty of Science, University Moulay Ismail, Meknes, Morocco; khalil.elkhatabi@edu.umi.ac.ma (K.E.); mohx20@gmail.com (R.E); hajiilima@gmail.com (H.H.) a.ajanamohammed@fs.umi.ac.ma (M.A.A.); tahar.lakhlifi@yahoo.fr (T.L.); bouachrine@gmail.com (M.B.);
[2] Molecular Signaling & Drug Discovery Laboratory, Department of Biochemistry, Central University of Punjab, Bathinda, 151401, India; atul.kumarphd@cup.ac.in (A.K.S.); shashankbiochemau@gmail.com (S.K.);
[3] EST Khenifra, Sultan Moulay Sliman University, Beni mellal, Morocco; bouachrine@gmail.com (M.B.);
* Correspondence: khalil.elkhatabi@edu.umi.ac.ma (K.E.); shashankbiochemau@gmail.com (S.K.);
Scopus Author ID 57216557017 (K.E.)
55749344800 (S.K.)
Received: 29.11.2021; Accepted: 30.12.2021; Published: 6.02.2022

Abstract: The α-amylase is regarded as a promising drug target for diabetes mellitus-type II. Hence, inhibiting α-amylase activity is a potential drug discovery approach for treating this chronic metabolic disorder. The present study explores the structural requirements and understands the inhibition mechanism of the novel developed indole-based derivatives as α-amylase inhibitors through 3D-QSAR, molecular docking, ADMET, and molecular dynamics (MD) simulation. The 3D-QSAR study showed good statistical reliability for two developed predictive models; CoMFA and CoMSIA. Through a deep investigation of docking analysis, detailed interactions with α-amylase of the most active compound 7 were explored. Four new indole derivatives were designed based on the contour maps and docking analysis, with significantly higher inhibitory activity than the molecules in the dataset. The selected molecules were evaluated for pharmacokinetic properties, showing a reasonably good ADMET profile. Furthermore, a 20-ns MD simulation of selected compounds bound to α-amylase was performed to ensure stability during simulation further. Greater stability of the designed molecule-protein complex A1 was found. The present findings shed light on the binding mode and the interactions between newly designed compounds, especially compound A1 and α-amylase and may be beneficial for drug development efforts targeting type-II diabetes.

Keywords: type 2 diabetes; α-amylase; indole; molecular docking; molecular dynamics simulation; *in silico* ADMET.

1. Introduction

Diabetes mellitus is a serious problem that threatens human health worldwide [1]. It is known to be one of the most common causes of death worldwide. It aggravates the rise of cardiovascular ailments and microvascular complications such as nephropathy, peripheral neuropathy, and retinopathy [2]. DM is characterized by hyperglycemia caused by a defect in insulin's action and/or secretion [3]. Among the two major types (Type I and II) of DM, Type I is diagnosed in 90% of DM cases [4,5]. Diabetes that is induced by complete insulin

deficiency is identified as type-I. In contrast, impaired insulin secretion leads to type-2 as a consequence of genetic susceptibility, physical inactivity, and excess body weight [6]. Diabetes mellitus (type II) can be effectively treated with α-amylase inhibitors, which efficiently control and reduce postprandial hyperglycemia [7]. α-amylase is a protein enzyme EC.3.2.1.1 that lies under the glycoside hydrolase family and is found in pancreatic saliva and juice [8,9]. It facilitates the breakdown of polysaccharides into glucose (absorbable monosaccharides) and maltose and targets the control of blood glucose levels [10]. α-amylase is an enzyme that acts to hold postprandial hyperglycemia under regulation [11]. Meanwhile, synthetic oral hyperglycemic drugs (acarbose and miglitol), which are α-amylase inhibitors, usually cause several side effects on the human body, like bellyache, flatulence, diarrhea, and abdominal distension [12]. Therefore, it is necessary to target the α-amylase enzyme, which is responsible for the digestion of carbohydrates, by developing new effective and safe therapeutic agents with low toxicity and high activity for the management of diabetes [13]. Among heterocyclic nitrogen compounds, the indole moiety has several pharmacological and medical potentials. It thus has motivated chemists to search for new potential lead molecules and their pharmacological properties with minor or no side effects [14]. Indole has emerged as an important pharmacophore for diabetes mellitus treatment, particularly as an α-amylase inhibitor. In addition, indole and its derivatives are endowed with various biological activities, such as cytotoxic, antimalarial, antimicrobial, anti-inflammatory, and anticancer [15–18].

In the pharmaceutical industry, discovering new drugs is a lengthy process. Hence, several computational techniques have dramatically decreased the overall cost and time of drug discovery. Computational studies have shown outstanding findings in the drug design process [19,20]. The 3D-QSAR, docking, and pharmacokinetic properties (ADMET) have served as valuable computational tools for drug discovery and development [21]. 3D-QSAR, including CoMFA and CoMSIA and docking together, proposed key elements and contributed to structural modification to develop new α-amylase inhibitors having increased potency [22]. *In silico* ADMET prediction of lead candidates helps evaluate the pharmacokinetic properties of molecules [23]. A molecular dynamics study was conducted to analyze conformational changes and evaluate the stability of the selected complexes [24]. The present study has been designed to rationally design and develop new α-amylase inhibitors as potential candidates using a computer-based drug design approach for further *in vitro* studies and evaluations.

2. Materials and Methods

2.1. Prepared database.

For the 3D-QSAR study, thirty-four indole-based derivatives with their associated α-amylase inhibitory activity IC_{50} were used as a data set based on literature studies [25,26]. *In vitro* activities, IC_{50} (uM) were converted into pIC_{50} values. The series was split into two parts: a training set of 26 compounds for model generation and a test set of 8 compounds for model validation. The structures of molecules and associated pIC_{50} values are listed in Table 1.

2.2. Geometry optimization and molecular alignment.

The three-dimensional (3D) structure of the indole derivatives was sketched using the Sybyl X-2.0 program (Tripos Inc., St. Louis, USA) and subsequently optimized under the Tripos standard force field with 0.01 kcal/mol Å as a convergence criterion [27]. Gasteiger-

Hückel charges were added to the compounds by the Powell method [28]. Default values were used for all other parameters.

Table 1. Chemical structures and α-amylase activities pIC_{50} of indole-based derivatives.

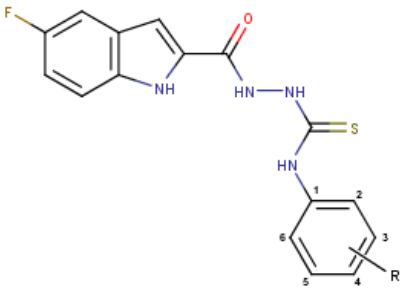

1-18

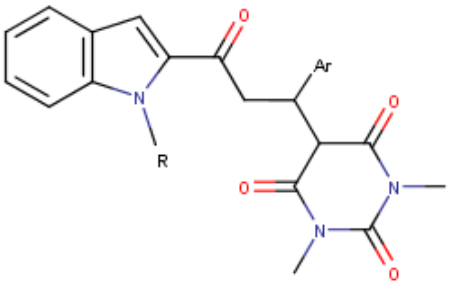

19-34

N°	R	Ar	pIC_{50}	N°	R	Ar	pIC_{50}
1	4-CF_3	-	4.796	**18**	6-OMe	-	4.428
2*	H	-	4.229	**19**	Me	Ph	4.030
3*	4-Br	-	4.674	**20**	Et	4-MePh	4.096
4	3-Br	-	4.501	**21**	Et	4-ClPh	4.147
5	3-Br, 4-Me	-	4.367	**22**	Et	2,4-Cl_2Ph	4.016
6	4-OMe	-	4.474	**23**	Et	4-OMePh	4.053
7	2-F	-	4.881	**24***	Et	4-BrPh	4.107
8	4- Me	-	4.415	**25***	Et	4-FPh	4.063
9	4-F	-	4.849	**26**	Et	3-FPh	4.048
10*	5-F	-	4.576	**27**	Et	3-MePh	4.021
11	4-Cl	-	4.798	**28***	Et	3-BrPh	4.063
12	2-Cl	-	4.587	**29**	Et	4-CF_3Ph	4.327
13	3-Cl	-	4.529	**30**	Et	Thiophinyl	4.451
14	2-Br	-	4.453	**31***	Et	Furanyl	4.085
15	2- Me	-	4.326	**32**	Et	3,4,5-OMe_3Ph	4.030
16	3- Me	-	4.402	**33**	Et	2-Napthyl	4.663
17*	3-OMe	-	4.455	**34**	Et	4-NO_2Ph	4.201

* Test set molecules

The optimization of the studied compounds was done using the DFT method with a basic set of B3LYP/6.311 (d, p) levels to achieve the equilibrium geometry of each [29]. The optimization was performed using Gaussian software (09, Gaussian Inc., Wallingford, CT, USA). Molecular alignment plays a substantial role in generating reliable QSAR models [30]. Superimposing of data set molecules was performed based on the common substructure, 1H-indole-2-carbaldehyde, using the most active compound **7** as a template, as depicted in Figure 1. The Align Database command in Sybyl was used for the alignment [31].

A **B**

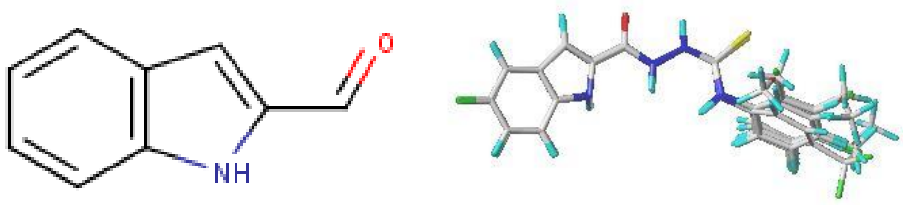

Figure 1. A. Common core used for alignment; **B**. Alignment of all molecules using compound 7 as a template.

2.3. CoMSIA and CoMFA.

As the accuracy of 3D-QSAR models relies mainly on molecular alignment, the alignment of compounds was carried out on database compounds by using compound **7** as a

representative template [32,33]. The Comparative Molecular Field Analysis (CoMFA) and Comparative Molecular Similarity Indices Analysis (CoMSIA) methods were developed upon the alignment to correlate the inhibitory activity of molecules' training set and their structures [34,35]. In a 3D cubic lattice with a regularly spaced grid of 2Å, the potential molecular fields between each molecule and a probe atom were calculated. The steric and electrostatic fields were determined in the CoMFA fields. In addition to steric and electrostatic fields, hydrogen bond acceptor and donor and hydrophobic fields were also calculated in the CoMSIA field at each lattice. 3D-QSAR studies were achieved in standard settings; the minimum sigma (column filtering) was set at 2.0 kcal/mol, and the energy cutoff value was 30 kcal/mol [36]. Therefore, the contour maps of CoMFA and CoMSIA were generated to visualize the field effects on the target feature [37].

2.4. Partial least square (PLS) analysis.

The PLS method is a statistical approach that generates statistically significant 3D-QSAR models and identifies a linear relationship by correlating the changes in the structures (independent variables) with their biological activity values as dependent variables [36]. PLS analysis with leave-one-out cross-validation determined the cross-validation correlation coefficient (Q^2), which is considered as a statistical index of internal predictability, and the optimum number of components (N). Moreover, the correlation coefficient (R^2), the Fisher test (F), and standard error of estimate (SEE) values were obtained by non-cross-validated analysis to assess the reliability of the developed models. The general conditions ($Q^2 > 0.50$ and $R^2 > 0.60$) [38,39], low SEE value, and an optimal number of components must be satisfied for a predictive QSAR model. Furthermore, external validation is carried out using a test set of molecules to evaluate the external predictability of the developed models. The value of r_{ext}^2 should fall between 0.6 and 1. Generated 3D-QSAR models with acceptable statistical values were selected [40,41].

2.5. Molecular docking.

Molecular docking is an efficient approach for investigating the binding characteristics of indole derivatives with the enzyme and identifying important active site residues via Surflex-Dock [42–44]. Consequently, the Total-Score, which represents the binding force, was generated. The higher Total-Score strongly denotes powerful binding affinity, which was subsequently chosen as the docking outcome. The results were analyzed using PyMol and Discovery studio 2016 software [45,46]. The crystal structure of the α-amylase enzyme (PDB code: 4UAC) was utilized for this study. The protein was prepared by adding Kohlman charges and polar hydrogens and removing water molecules from the receptor using Discovery Studio software. Finally, the active ligand of the studied compounds and proposed ligands were energetically minimized and geometrically optimized using default parameters and then docked to the active site of α-amylase. Therefore, this method can effectively confirm the results obtained from the 3D-QSAR study.

2.6. ADMET prediction.

The ADMET prediction of compounds in advance at earlier stages is extremely advantageous for generating and evaluating good potential candidates in clinical trials. The

pharmacokinetic ADMET properties of the 5 selected indole-based derivatives were predicted using SwissADME and pKCSM web tools [47,48].

2.7. MD simulation.

Molecular dynamics simulations are widely used to understand biomolecular complexes' dynamic behavior and conformational changes [49,50]. The drug candidates complexed with the target protein were subjected to MD simulation to explore ligands' dynamic behavior and conformational changes [51]. The GROMACS 5.1.1 software package was utilized with the gromos54a7 force field to execute 20 nanosecond MD simulations on docked inhibitor-protein complexes [52]. The PRODRG server [53] was used to generate ligand parameters using the same force field. The dodecahedron simulation box was generated by gmx editconf tool. Using the gmx solvate tool, the system was solvated with the SPC water model. The electro-neutralization of the system was performed using gmx genion tool. The structure was then optimized using energy minimization to avoid steric clashes. Equilibration was done in two steps after energy minimization. To stabilize the system's temperature, the NVT equilibration was performed at 300 K for 100 picoseconds. Following that, a 100 picosecond NPT equilibration at 1 bar pressure was performed using the Parrinello-Rahman barostat and the LINear Constraint Solver (LINCS) algorithm with bond lengths conserved [54,55]. Long-distance electrostatic interactions were treated using Particle Mesh Ewald (PME) [56]. Finally, the 20 ns MD simulation was applied to each complex with the desired temperature and pressure on an HP desktop with a Linux operating system with Intel Core i-7 processor (32 GB RAM).

3. Results and Discussion

3.1. 3D-QSAR statistical results.

Statistical results calculated for COMFA and COMSIA models are summarized in Table2, while Figure 2 displays the relationship between observed and predicted pIC50 for training and test set compounds for CoMFA and CoMSIA. Both models were performed for the analysis with a training set of 26 Indole derivatives whose *in vitro* biological activities were reported as α-amylase inhibitors. The optimal CoMFA and CoMSIA models resulted in an optimized component model of 3 with cross-validated Q^2 of 0.657 and 0.677, respectively. While non-cross-validated R^2 for CoMFA and CoMSIA were 0.952 and 0.944, respectively, and low standard error (SEE), which was significant for good internal QSAR model prediction ability. External validation of the test set (8 compounds) produced r_{ext}^2 values of 0.832 and 0.827 for the CoMFA and COMSIA models, indicating good predictability for both models. The field contribution of steric and electrostatic for the CoMFA model accounted for 68.5% and 31.5%, respectively, while in the CoMSIA model, steric, electrostatic, H-bond donor, and hydrophobic were 16.1%, 46.6%, 1.5%, and 35.8%, respectively.

Table 2. Summary of statistical results.

Model	Q^2	R^2	SEE	F	N	r_{ext}^2	Fractions				
							Ster	Elect	Acc	Don	Hyd
CoMFA	0.657	0.952	0.041	61.37	3	0.832	0.685	0.315	-	-	-
CoMSIA	0.677	0.944	0.048	43.17	3	0.827	0.161	0.466	-	0.015	0.358

The scatter plots of the observed and predicted pIC_{50} for the data set compounds exhibit that all points are distributed near or close to the straight line. These findings imply that the derived models were of good quality.

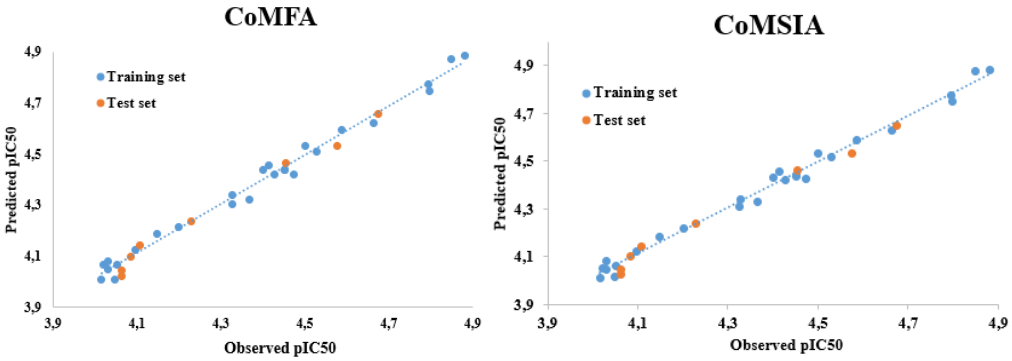

Figure 2. Plots of observed and predicted pIC50 for CoMFA and CoMSIA.

3.2. 3D-QSAR contour maps.

The contour maps were created to explicate the relationship between the structures of compounds and their associated activities, using compound **7** as a template. CoMFA and CoMSIA contour maps are shown in Figures 3 and 4, respectively. According to the structural features provided by the contour maps, the modification in certain regions would relate to biological activity change, which could be guided in designing new molecules with improved activity.

3.2.1. CoMFA contour maps.

As depicted in Figure 3A of the steric contour maps, sterically favorable and unfavorable interactions are shown as green (80% contribution) and yellow (20% contribution) contours, respectively, while in the electrostatic contour maps (Figure 3B), the red (20% contribution) contours refer to regions in which electronegative charges increase activity, whereas the blue (80% contribution) contours represent regions in which electropositive charges decrease activity.

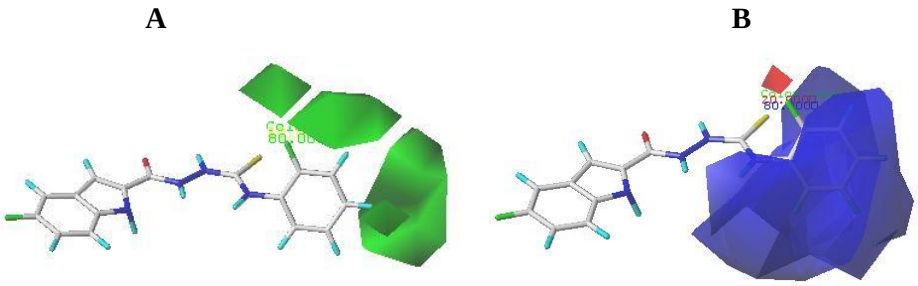

Figure 3. Contour maps of CoMFA analysis. **A.** Steric field; **B.** Electrostatic field.

Around the fourth position of the phenyl ring, a medium green-colored map indicating a bulky group is favored for improving potency. This finding is in line with the fact that the compounds **1**, **9,** and **11** with CF_3, F, and Cl substituents, respectively, exhibited excellent pIC_{50} values than compounds **2** and **8** with H and CH_3 groups, respectively. Two green contour maps appeared at the C-2 and C-3 positions of the same phenyl, indicating that bulkier groups at the corresponding positions would be favored for potency. This finding is also supported by

compounds **7** (-F) and **13** (-Cl) that show more potency than compounds **15** (–CH_3) and **16** (-CH_3). For the electrostatic field, a red contour is mapped close to C-2 of the phenyl ring, implying its preference for the electronegative groups at this position. This could be explained by the higher activity of compound **7** with the –F group than that of compound **18** holding –OMe group. Furthermore, a region with blue contours was found around the phenyl, with the exception of position C-2, which is covered by a small red contour, implying that compounds with electropositive groups at these positions should be more potent than those with no or electronegative groups.

3.2.2. CoMSIA contour maps.

Figure 4A was the contour map of the steric field of the CoMSIA model. This finding was fully consistent with the corresponding CoMFA model. For the electrostatic field (Figure 4B), a small red contour map is depicted near the fourth position of the phenyl ring, indicating that the electronegative group situated in this position will improve the potency, which the higher activity of compound 9 could demonstrate (pIC_{50} = 4.854) and compound **11** (pIC_{50} =4.803), with –F and-Cl at the C-4 position, respectively. Additionally, a blue contour was located inside the phenyl ring, which implied electropositive functional groups in this region would be advantageous for potency. Therefore, this finding is in line with observations obtained from the reference compound **7**, which systematically compared the effect of modification of the substitutes in this area. If the –F was substituted by OCH_3, the potency would be decreased.

Figure 4C clearly shows the hydrogen bond donor contour map. The cyan (80% contribution) and purple (20% contribution) contours representing favorable and unfavorable hydrogen-bond acceptors benefit the potency. The cyan contour located at the linker between the two rings suggested that H-bond donor functional groups at these positions could improve the α-amylase inhibitory activity. The change in substitutes was performed only on the phenyl ring. Consequently, there is no difference between compounds at this stage, considering the absence of the purple contour.

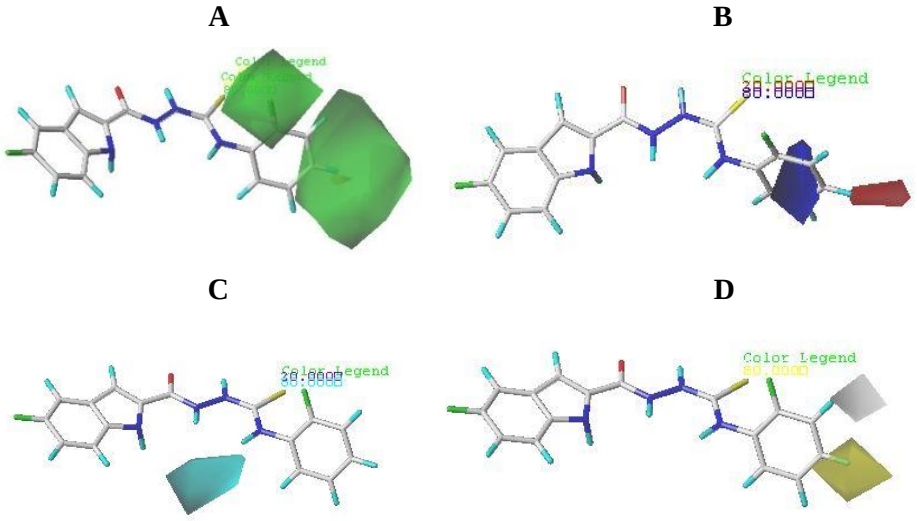

Figure 4. Contour maps of CoMSIA analysis. **A.** Steric field; **B.** Electrostatic field; **C.** H-bond acceptor field; **D.** Hydrophobic field.

The hydrophobic contour map is shown in Figure 4D. The yellow (80% contribution) contours and white (20% contribution) contours refer to hydrophobic favored and unfavorable areas for activity, respectively. The hydrophobic field contour shows that a yellow polyhedron

contour is depicted near the C-4 position, meaning that the addition of hydrophobic functional groups in this yellow area may increase the activity, exemplified by compounds **1** and **9**. At the same time, the presence of a white region near the C-3 position indicated that a hydrophilic group is favored in the overall activity. The electrostatic and hydrophobic interaction match well with the experimental results, which is useful for designing novel indole derivatives with improved α-amylase inhibitory activity.

3.3.3. Molecular docking.

Following QSAR analysis, α-amylase (PDB:4UAC) was molecularly docked with the most active compound in the data system and the designed molecules using the Surflex-docking method. Compound **7** was chosen for detailed analysis to analyze the binding mode between the receptor and inhibitor, as depicted in Figure 5. This enabled understanding the electrostatic, H-bonding, and hydrophobic interactions of the active molecule in the α-amylase active site. The docking scores of the selected compounds are listed in Table 3. The four designed compounds have electronegative groups (C=S; C=O) and electropositive groups (N; NH). This outcome is consistent with the electrostatic field, suggesting that the addition of proton donors or proton acceptors can inhibit the activity of an enzyme. Considering this result, the molecular docking study and α-amylase inhibitory assay revealed that compound **7** inhibits the α-amylase enzyme by interacting with SER87, ASN245, and ASN191 amino acid residues, forming hydrogen bonds with the inhibitors, which is very advantageous for binding.

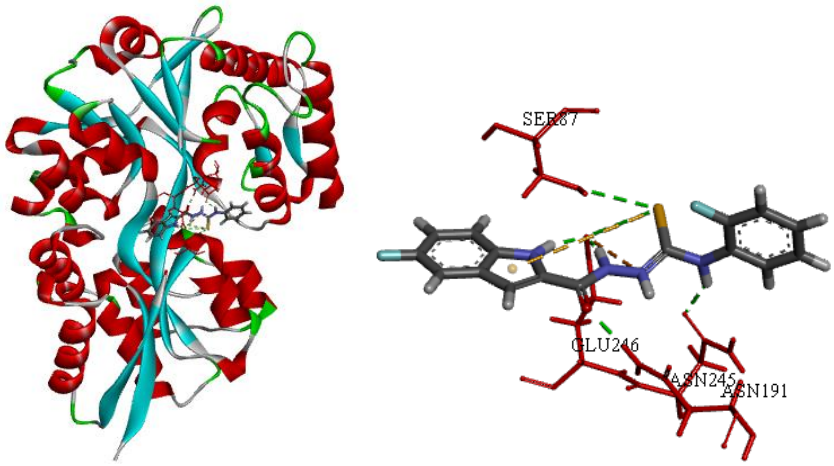

Figure 5. Docking pose of α-amylase with compound 7.

The representative compound binds closely to the target protein, as shown in Figure 6, based on further docking analysis. Furthermore, a rich electrostatic interaction was generated by the pocket between the ligand and the α-amylase receptor. The red italic color around position 4 of the phenyl ring indicates that a substituent with an electronegative character is favored in this position, which is in line with the results described through the analysis of CoMSIA electrostatic contour maps. Furthermore, from Figure 6, it is seen that the representative compound is accommodated in the hydrophilic pocket. The positions C-3 and C-5 were found in the blue area, which points out that introducing groups with hydrophilic characters here would greatly improve the stability of the binding. This observation implies that hydrophilic substituents might establish a stronger inhibitory potency on the α-amylase protein, which correlates with the above hydrophobic plot analysis (Figure 4C). As shown in Figure 6, the phenyl ring was stretched into the innermost H-bond donor and acceptor regions

of the active pocket. Positions C-2 and C-3 were found in the pink area, suggesting their affinity to H-bond donor substituents, while position 4 was covered by a green contour indicating that H-bond acceptor groups would benefit this position. This makes the docking complex conformation more stable. These results fully prove the reliable correlation of the developed models and guarantee the stability of the four designed α-amylase inhibitors.

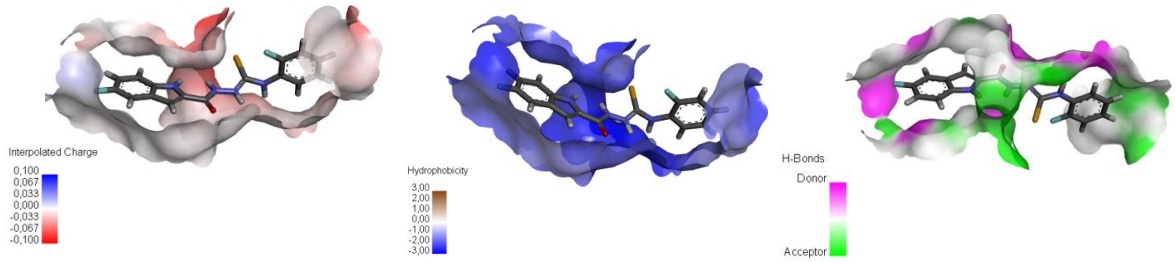

Figure 6. The interaction of electrostatics, hydrophobicity, and H-bond between the active molecule and 4UAC receptor.

3.3. Design and prediction.

By analyzing the structural features obtained from 3D-QSAR and molecular docking studies, the dominant modified area of the representative compound was modified. Consequently, four indole-based derivatives which showed potently predicted pIC_{50} values were designed and docked into the α-amylase substrate pocket. The newly designed derivatives **A1**, **A2**, **A3,** and **A4** exhibited exceptionally enhanced potency and possessed a higher Surflex-Dock Score than compound **7** for the established models, as shown in Table 3.

Table 3. Chemical structure and predicted pIC_{50} of newly designed molecules.

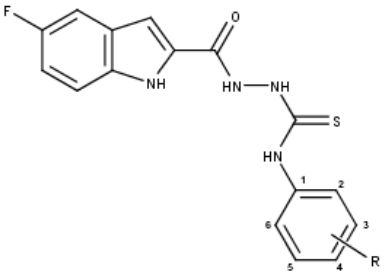

N°	Structure	Predicted pIC_{50}		Total Score
	R	CoMFA	CoMSIA	
Comp7	2-F	4.802	4.793	5.0378
A1	2-OCH_3,4-CF_3	4.926	4.941	7.1275
A2	2-OCH_3, 4-F	4.967	4.969	3.1852
A3	3,5-di-OH	4.887	4.890	4.7903
A4	3-OH, 4-F	4.824	4.824	4.7274

3.4. ADMET properties.

To further ensure the viability of the designed molecules, pharmacokinetic ADMET properties were also predicted via pkCSM. Therefore, the drug candidates **A1**, **A2**, **A3**, and **A4**, and compound **7** were chosen as the control group. The results of ADMET properties are reported in Table 4.

3.4.1. Absorption and distribution.

A molecule with less than 30% absorbance is labeled as poorly absorbed by the human enteric system. For all tested compounds, the percentage of human oral absorption ranged from

72.806 to 90.891%, which indicates that all tested compounds were considered well absorbed. The volume of distribution (VDss) value logVDss below -0.15 signifies poor distribution. All designed compounds displayed >-0.15 VDss value. In contrast, the most active compound displayed a value below -0.15, which reveals that the designed compounds have the ability to be distributed in tissues rather than plasma.

3.4.2. Metabolism.

The enzymatic metabolism plays a significant role in converting a substance, such as a drug, which points out the biotransformation of a drug within the body. As can be seen in Table 4, all tested compounds were found to be CYP3A4 substrates. However, the tested molecules were found to inhibit the two main subtypes, CYP2D6 and CYP3A4 of cytochrome P450, which means that they might have the ability to be metabolized in the liver.

3.4.3. Excretion and toxicity.

The tested molecules show somewhat low values of total clearance but are still acceptable, which could be filtered by renal and hepatic tissues in a combinational way. They were further evaluated for the Ames toxicity test. The analysis showed a negative result, indicating that none of these compounds were mutagenic or presented a risk of carcinogenicity, indicating the safety of the compounds, which is extremely advantageous for the development of an active drug.

The ADMET analysis indicated that the newly designed compounds were verified *in silico* and might be used as safer lead compounds in future research. For the following simulation, we selected Compound **A1** among the newly designed molecules to study the stability and compare it to that of the most active molecule **7** in the studied system to support its use as a novel α-amylase inhibitor.

Table 4. Pharmacokinetic (ADMET) properties of newly designed compounds.

	Absorption	**Distribution**	**Metabolism CYP**							**Excretion**	**Toxicity**	
	Intestinal Absorption (human) (%absorbed)	VDss (human) (logL/Kg)	2D6	3A4	1A2	2C19	2C9	2D6	3A4	Total Clearance ((logmL/min/kg)	AMES	Carcinogens
			Substrate		Inhibitor							
Most active compound from the studied dataset												
Comp7	90.891	-0.452	Yes	No	Yes	Yes	Yes	No	No	-0.424	No	No
Newly designed compounds												
A1	86.785	0.029	Yes	No	Yes	Yes	Yes	No	No	-0.263	No	No
A2	90.142	0.151	Yes	No	Yes	Yes	Yes	No	No	-0.273	No	No
A3	72.806	-0.215	Yes	No	Yes	Yes	Yes	No	No	-0.354	No	No
A4	87.016	0.049	Yes	No	Yes	Yes	Yes	No	No	-0.518	No	No

VDss: volume of distribution at steady state. CYP: cytochrome P450. AMES: bacterial reverse mutation.

3.5. MD simulation.

The 3D-crystal structure of α-amylase protein docked with selected compounds was further subjected to 20 ns MD simulations that were performed to investigate the comparative conformation dynamics of the protein after ligand binding [57,58]. During the 20-ns simulation, the compound-bound protein's temperature, pressure, and energy parameters remained stable. (Figure 7A, 7B, 7C and 7D). Table 5 shows the average values of various MD-related properties.

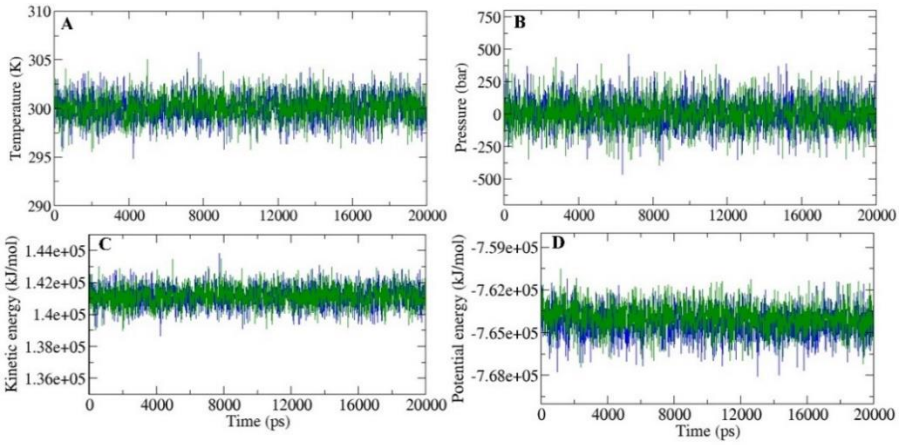

Figure 7. A. Temperature of the target protein complexed with the active (Blue) and designed molecule (Green). **B.** The pressure of the target protein is complexed with the active (Blue) and designed molecule (Green). **C.** Kinetic energy of target protein complexed with active (Blue) and designed molecule (Green). **D.** Potential energy of target protein complexed with the active molecule (Blue) and designed molecule (Green).

Table 5. Average values of molecular dynamics simulation parameters during 20 ns period.

Parameter	Active molecule complex	Designed molecule complex A1
RMSD	0.2873 ± 0.0453	0.3021 ± 0.0471
RMSF	0.1172 ± 0.0537	0.1440 ± 0.0726
Radius of gyration	2.1674 ± 0.0115	2.150 ± 0.0128
SASA	200.3689 ± 1.7430	200.3724 ± 2.6384
Intra-Protein Hydrogen bonds	308.6552 ± 8.5965	307.3333 ± 8.8598
Protein solvent hydrogen bonds	737.6632 ± 18.5614	724.3758 ± 19.9896

The root-mean-square deviation (RMSD) calculates the average distance between the atoms (e.g., backbone atoms of a protein) throughout the simulation. RMSD analysis provides information about the conformational stability as well as the equilibrium of the protein-ligand, ligand, and unbound protein systems during simulation. The average values of backbone RMSD for protein-active molecule complex and protein-designed molecule complex were 0.2873 ± 0.0453 nm and 0.3021 ± 0.0471 nm, respectively (Figure 8A). The RMSD analysis of both complexes shows that the RMSD of the protein-designed molecule complex is similar during the 20 ns MD simulation. Next, we calculated the root mean square fluctuation (RMSF) to analyze the effect of the active molecule and designed molecule binding on the internal dynamics of the target protein (Figure 8B). The average RMSF values for protein-active and protein-designed complexes were 0.1172 ± 0.0537 nm and 0.1440 ± 0.0726 nm, respectively. RMSF analysis indicated that the binding of the designed molecule to the target protein resulted in slightly more fluctuations in comparison to the binding of the active molecule. The radius of gyration (Rg) provides insight into the deviation in the compactness of protein structure and evaluates the folding of regular secondary structures into the protein's three-dimensional structure. The effect of the active molecule and designed molecule binding on the gyration radius value of the protein was calculated (Figure 9A). Average Rg values for protein-active molecule complex and protein-designed molecule complex were 2.1674 ± 0.0115 nm and 2.150 ± 0.0128 nm, respectively. Rg analysis reveals that the compactness of folding of the target protein after binding both the active molecule and the designed molecule is not significantly different. The bimolecular surface area assessable to surrounding solvent molecules is determined by the solvent-accessible surface area (SASA). The change in SASA for protein-active molecule complex and protein-designed molecule complex were analyzed (Figure 9B). Average values of SASA for protein-active molecule complex and protein-designed molecule

complex were reported as 200.3689 ± 1.7430 nm^2 and 200.3724 ± 2.6384 nm^2, respectively. Analysis of SASA shows that both the complexes have similar SASA values.

Hydrogen bonds formation is important in stabilizing the structure of protein and ligand-protein complexes since it minimizes the system's energy. Intra-protein (Figure 10A) solvent-protein and ligand-protein hydrogen bonding patterns were studied in both complexes (Figure 10B, 10C, and 10D). The average values of intra-protein hydrogen bond in protein-active molecule complex and protein-designed molecule complex were 308.6552 ± 8.5965 and 307.3333 ± 8.8598, respectively. Furthermore, active molecule bound protein formed 737.6632 ± 18.5614 hydrogen bonds with the solvent compared to 724.3758 ± 19.9896 hydrogen bonds formed by designed molecule bound protein. The formation of hydrogen bonds between target protein-active molecule (Figure 10C) and target protein-designed molecule (Figure 10D) was also studied. The designed molecule formed slightly more hydrogen bonds with the target protein than the active molecule, which indicates the strong binding activity of the designed molecule. There were no significant changes in secondary structure observed upon binding of both molecules.

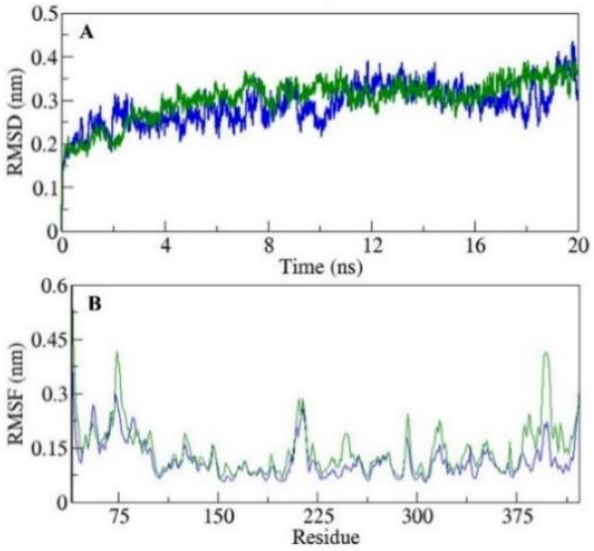

Figure 8. A. Backbone RMSD of the target protein with the active (Blue) and designed molecule (Green).**B.** RMSF of the target protein with the active (Blue) and designed molecule (Green).

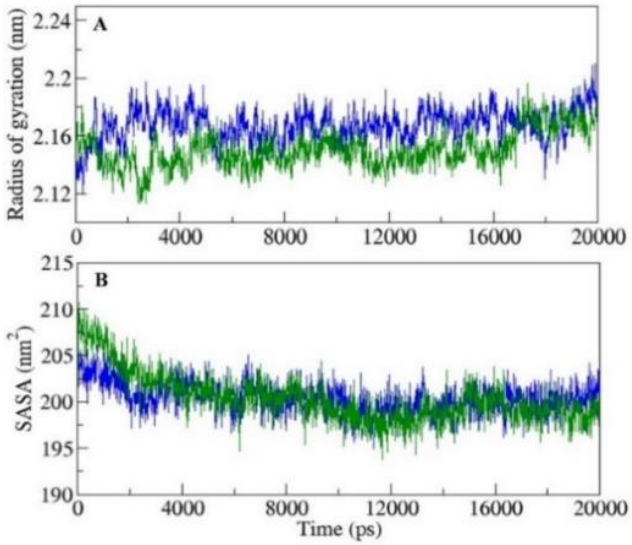

Figure 9. A. Radius of gyration (Rg) of the target protein with the active (Blue) and designed molecule (Green). **B.** SASA of the target protein with the active (Blue) and designed molecule (Green).

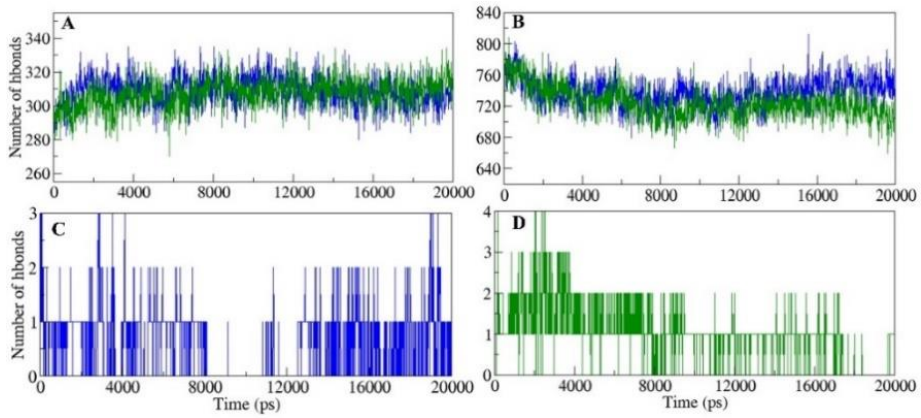

Figure 10. A. Intra-protein hydrogen bond formation in the target protein with the active (Blue) and designed molecule (Green). **B.** Hydrogen bond formation between the target protein and surrounding water molecules in active (Blue) and designed molecule complexed (Green) with the protein C**.** Hydrogen bond formation between protein complexed with the active molecule. **D.** Hydrogen bond formation in protein and designed molecule complex.

4. Conclusion

A ligand-based pharmacophore was performed in combination with docking analysis and MD simulation to design new α-amylase inhibitors targeting type-II diabetes. The 3D-QSAR technique was executed to statistically study the relationship between structure and activity of reported indole inhibitors. Using an internal validation test set, reliable CoMFA and CoMSIA models were generated and validated, evident from Q^2 and R^2 values. The developed models were also validated using a test set of molecules, indicating good predictability. Moreover, molecular docking was applied to analyze the interaction characteristics between ligands and α-amylase, which were in good accordance with the chemical features of indole unveiled by the contour maps analysis. These findings were extremely helpful in developing four new inhibitors with higher affinities targeting α-amylase, among which compound **A1** exhibited higher predicted activity and docking score.

Furthermore, each designed compound has been subjected to standard computational pharmacokinetic ADMET parameters to evaluate the drug-like ability. Moreover, the molecular dynamics simulation process of the newly designed compound **A1** was established to study the dynamic behavior and check the conformational stability at the binding site of α-amylase. The mentioned results support the potential of compound **A1** to be further developed as a novel α-amylase inhibitor able to treat type-II diabetes.

Funding

This research received no external funding.

Acknowledgments

We are grateful to the "Association Marocaine des Chimistes Théoriciens" (AMCT) for its pertinent help concerning the programs. SK acknowledges the Department of Science and Technology, India, for providing financial support in the DST-SERB Grant (EEQ-2016/00350) and the Department of Biochemistry, DST-FIST Grants. AKS acknowledges the Council of Scientific and Industrial Research, India, for providing the Senior Research Fellowship (File.No:99/1051(0014)/2018-EMR-I).

Conflicts of Interest

The authors declare that they have no conflict interests.

References

1. Lee, C.-C.; Hsing, S.-C.; Lin, Y.-T.; Lin, C.; Chen, J.-T.; Chen, Y.-H.; Fang, W.-H. The Importance of Close Follow-Up in Patients with Early-Grade Diabetic Retinopathy: A Taiwan Population-Based Study Grading via Deep Learning Model. *Int. J. Environ. Res. Public. Health* **2021**, *18*, 9768, https://doi.org/10.3390/ijerph18189768.
2. Rahim, F.; Zaman, K.; Taha, M.; Ullah, H.; Ghufran, M.; Wadood, A.; Rehman, W.; Uddin, N.; Shah, S. A. A.; Sajid, M.; Nawaz, F.; Khan, K. M. Synthesis, *in vitro* Alpha-Glucosidase Inhibitory Potential of Benzimidazole Bearing Bis-Schiff Bases and Their Molecular Docking Study. *Bioorganic Chem.* **2020**, *94*, 103394, https://doi.org/10.1016/j.bioorg.2019.103394.
3. Imran, S.; Taha, M.; Selvaraj, M.; Ismail, N. H.; Chigurupati, S.; Mohammad, J. I. Synthesis and Biological Evaluation of Indole Derivatives as α -Amylase Inhibitor. *Bioorganic Chem.* **2017**, *73*, 121–127, https://doi.org/10.1016/j.bioorg.2017.06.007.
4. Kalra, S.; Bantwal, G.; Kapoor, N.; Sahay, R.; Bhattacharya, S.; Anne, B.; Gopal, R. A.; Kota, S.; Kumar, A.; Joshi, A.; Sanyal, D.; Tiwaskar, M.; Das, A. K. Quantifying Remission Probability in Type 2 Diabetes Mellitus. *Clin. Pract.* **2021**, *11*, 850–859, https://doi.org/10.3390/clinpract11040100.
5. Alam, S.; Hasan, M. K.; Neaz, S.; Hussain, N.; Hossain, M. F.; Rahman, T. Diabetes Mellitus: Insights from Epidemiology, Biochemistry, Risk Factors, Diagnosis, Complications and Comprehensive Management. *Diabetology* **2021**, *2*, 36–50, https://doi.org/10.3390/diabetology2020004.
6. Ramírez-Espinosa, J. J.; Rios, M. Y.; López-Martínez, S.; López-Vallejo, F.; Medina-Franco, J. L.; Paoli, P.; Camici, G.; Navarrete-Vázquez, G.; Ortiz-Andrade, R.; Estrada-Soto, S. Antidiabetic Activity of Some Pentacyclic Acid Triterpenoids, Role of PTP–1B: *In vitro*, *in silico*, and *in vivo* Approaches. *Eur. J. Med. Chem.* **2011**, *46*, 2243–2251, https://doi.org/10.1016/j.ejmech.2011.03.005.
7. Blahova, J.; Martiniakova, M.; Babikova, M.; Kovacova, V.; Mondockova, V.; Omelka, R. Pharmaceutical Drugs and Natural Therapeutic Products for the Treatment of Type 2 Diabetes Mellitus. *Pharmaceuticals* **2021**, *14*, 806, https://doi.org/10.3390/ph14080806.
8. R Rodríguez-Viera, L.; Alpízar-Pedraza, D.; Mancera, J. M.; Perera, E. Toward a More Comprehensive View of α-Amylase across Decapods Crustaceans. *Biology* **2021**, *10*, 947, https://doi.org/10.3390/biology10100947.
9. Li, H.; Zhou, H.; Zhang, J.; Fu, X.; Ying, Z.; Liu, X. Proteinaceous α-Amylase Inhibitors: Purification, Detection Methods, Types and Mechanisms. *Int. J. Food Prop.* **2021**, *24*, 277–290, https://doi.org/10.1080/10942912.2021.1876087.
10. Taha, M.; Irshad, M.; Imran, S.; Rahim, F.; Selvaraj, M.; Almandil, N. B.; Mosaddik, A.; Chigurupati, S.; Nawaz, F.; Ismail, N. H.; Ibrahim, M. Thiazole Based Carbohydrazide Derivatives as *α* -Amylase Inhibitor and Their Molecular Docking Study. *Heteroat. Chem.* **2019**, *2019*, 1–8, https://doi.org/10.1155/2019/7502347.
11. Tang, H.; Ma, F.; Zhao, D.; Xue, Z. Exploring the Effect of Salvianolic Acid C on α-Glucosidase: Inhibition Kinetics, Interaction Mechanism and Molecular Modelling Methods. *Process Biochem.* **2019**, *78*, 178–188, https://doi.org/10.1016/j.procbio.2019.01.011.
12. Li, C.; Hung, Y.-J.; Qamruddin, K.; Aziz, M. F. A.; Stein, H.; Schmidt, B. International Noninterventional Study of Acarbose Treatment in Patients with Type 2 Diabetes Mellitus. *Diabetes Res. Clin. Pract.* **2011**, *92*, 57–64, https://doi.org/10.1016/j.diabres.2010.12.033.
13. Gad-Elkareem, M. A. M.; Abdelgadir, E. H.; Badawy, O. M.; Kadri, A. Potential Antidiabetic Effect of Ethanolic and Aqueous-Ethanolic Extracts of *Ricinus Communis* Leaves on Streptozotocin-Induced Diabetes in Rats. *PeerJ* **2019**, *7*, e6441, https://doi.org/10.7717/peerj.6441.
14. Cacchi, S.; Fabrizi, G. Synthesis and Functionalization of Indoles Through Palladium-Catalyzed Reactions †. *Chem. Rev.* **2005**, *105*, 2873–2920, https://doi.org/10.1021/cr040639b.
15. Liew, L. P. P.; Fleming, J. M.; Longeon, A.; Mouray, E.; Florent, I.; Bourguet-Kondracki, M.-L.; Copp, B. R. Synthesis of 1-Indolyl Substituted β-Carboline Natural Products and Discovery of Antimalarial and Cytotoxic Activities. *Tetrahedron* **2014**, *70*, 4910–4920, https://doi.org/10.1016/j.tet.2014.05.068.

16. Sharma, S. K.; Kumar, P.; Narasimhan, B.; Ramasamy, K.; Mani, V.; Mishra, R. K.; Majeed, A. B. A. Synthesis, Antimicrobial, Anticancer Evaluation and QSAR Studies of 6-Methyl-4-[1-(2-Substituted-Phenylamino-Acetyl)-1H-Indol-3-Yl]-2-Oxo/Thioxo-1,2,3,4-Tetrahydropyrimidine-5-Carboxylic Acid Ethyl Esters. *Eur. J. Med. Chem.* **2012**, *48*, 16–25, https://doi.org/10.1016/j.ejmech.2011.11.028.
17. Mehndiratta, S.; Hsieh, Y.-L.; Liu, Y.-M.; Wang, A. W.; Lee, H.-Y.; Liang, L.-Y.; Kumar, S.; Teng, C.-M.; Yang, C.-R.; Liou, J.-P. Indole-3-Ethylsulfamoylphenylacrylamides: Potent Histone Deacetylase Inhibitors with Anti-Inflammatory Activity. *Eur. J. Med. Chem.* **2014**, *85*, 468–479, https://doi.org/10.1016/j.ejmech.2014.08.020.
18. Shaveta; Singh, P. Structural Optimization of Indole Based Compounds for Highly Promising Anticancer Activities: Structure Activity Relationship Studies and Identification of Lead Molecules. *Eur. J. Med. Chem.* **2014**, *74*, 440–450, https://doi.org/10.1016/j.ejmech.2013.12.047.
19. Gurung, A. B.; Ali, M. A.; Lee, J.; Farah, M. A.; Al-Anazi, K. M. An Updated Review of Computer-Aided Drug Design and Its Application to COVID-19. *BioMed Res. Int.* **2021**, *2021*, 8853056, https://doi.org/10.1155/2021/8853056.
20. Sarvagalla, S.; Syed, S. B.; Coumar, M. S. An Overview of Computational Methods, Tools, Servers, and Databases for Drug Repurposing. In *In silico Drug Design*; Elsevier, 2019; 743–780, https://doi.org/10.1016/B978-0-12-816125-8.00025-0.
21. Singh, A. K.; Kushwaha, P. P.; Prajapati, K. S.; Shuaib, M.; Gupta, S.; Kumar, S. Identification of FDA Approved Drugs and Nucleoside Analogues as Potential SARS-CoV-2 A1pp Domain Inhibitor: An *in silico* Study. *Comput. Biol. Med.* **2021**, *130*, 104185, https://doi.org/10.1016/j.compbiomed.2020.104185.
22. El Khatabi, K.; Aanouz, İ.; El-Mernissi, R.; Khaldan, A.; Ajana, M. A.; Bouachrine, M.; Lakhlifi, T. Designing of Novel Potential Inhibitors of A-Amylase by 3D-QSAR Modeling and Molecular Docking Studies. *J. Turk. Chem. Soc. Sect. Chem.* **2020**, 469–478, https://doi.org/10.18596/jotcsa.703026.
23. Alaouy, M. A. E.; Youness, M.; Boutalaka, M.; Elbouhi, M.; Elmernissi, R.; Sbai, A.; Lakhlifi, T.; Bouachrine, M. The 2D-QSAR Study, Drug Likeness and in-Silico ADMET Prediction of about 3,5-Diaryl-1H-Pyrazole Derivatives as Multifunctional Agents for the Treatment of Alzheimer's Disease. *RHAZES Green Appl. Chem.* **2021**, *13*, 09–28, https://doi.org/10.48419/IMIST.PRSM/rhazes-v13.28095.
24. Hirano, Y.; Okimoto, N.; Fujita, S.; Taiji, M. Molecular Dynamics Study of Conformational Changes of Tankyrase 2 Binding Subsites upon Ligand Binding. *ACS Omega* **2021**, *6*, 17609–17620, https://doi.org/10.1021/acsomega.1c02159.
25. Kawde, A.-N.; Taha, M.; Alansari, R. S.; Almandil, N. B.; Anouar, E. H.; Uddin, N.; Rahim, F.; Chigurupati, S.; Nawaz, M.; Hayat, S.; Ibrahim, M.; Elakurthy, P. K.; Vijayan, V.; Morsy, M.; Ibrahim, H.; Baig, N.; Khan, K. M. Exploring Efficacy of Indole-Based Dual Inhibitors for α-Glucosidase and α-Amylase Enzymes: *In silico*, Biochemical and Kinetic Studies. *Int. J. Biol. Macromol.* **2020**, *154*, 217–232, https://doi.org/10.1016/j.ijbiomac.2020.03.090.
26. Badria, F. A.; Atef, S.; Al-Majid, A. M.; Ali, M.; Elshaier, Y. A. M. M.; Ghabbour, H. A.; Islam, M. S.; Barakat, A. Synthesis and Inhibitory Effect of Some Indole-Pyrimidine Based Hybrid Heterocycles on A-Glucosidase and A-Amylase as Potential Hypoglycemic Agents. *ChemistryOpen* **2019**, *8*, 1288–1297, https://doi.org/10.1002/open.201900240.
27. Clark, M.; Cramer, R. D.; Van Opdenbosch, N. Validation of the General Purpose Tripos 5.2 Force Field. *J. Comput. Chem.* **1989**, *10*, 982–1012, https://doi.org/10.1002/jcc.540100804.
28. Purcell, W. P.; Singer, J. A. A Brief Review and Table of Semiempirical Parameters Used in the Hueckel Molecular Orbital Method. *J. Chem. Eng. Data* **1967**, *12*, 235–246, https://doi.org/10.1021/je60033a020.
29. Lee, C.; Yang, W.; Parr, R. G. Development of the Colle-Salvetti Correlation-Energy Formula into a Functional of the Electron Density. *Phys. Rev. B* **1988**, *37*, 785–789, https://doi.org/10.1103/PhysRevB.37.785.
30. El Khatabi, K.; Aanouz, I.; El-Mernissi, R.; Khaldan, A.; Ajana, M. A.; Bouachrine, M.; Lakhlifi, T. 3D-QSAR and Molecular Docking Studies of p-Aminobenzoic Acid Derivatives to Explore the Features Requirements of Alzheimer Inhibitors. *Orbital Electron. J. Chem.* **2020**, *12*, 172–181, https://doi.org/10.17807/orbital.v12i4.1467.
31. El Khatabi, K.; El-Mernissi, R.; Aanouz, I.; Ajana, M. A.; Lakhlifi, T.; Khan, A.; Wei, D.-Q.; Bouachrine, M. Identification of Novel Acetylcholinesterase Inhibitors through 3D-QSAR, Molecular Docking, and Molecular Dynamics Simulation Targeting Alzheimer's Disease. *J. Mol. Model.* **2021**, *27*, 302, https://doi.org/10.1007/s00894-021-04928-5.

32. Khaldan, A.; Bouamrane, S.; En-Nahli, F.; El-Mernissi, R.; El Khatabi, K.; Hmamouchi, R.; Maghat, H.; Ajana, M. A.; Sbai, A.; Bouachrine, M.; Lakhlifi, T. Prediction of Potential Inhibitors of SARS-CoV-2 Using 3D-QSAR, Molecular Docking Modeling and ADMET Properties. *Heliyon* **2021**, *7*, e06603, https://doi.org/10.1016/j.heliyon.2021.e06603.
33. EL-Mernissi, R.; EL Khatabi, K.; Khaldan, A.; El Mchichi, L.; Ajana, M. A.; Lakhlifi, T.; Bouachrine, M. Design of New 3, 5-Disubstituted Indole as Hematological Anticancer Agents Using 3D-QSAR, Molecular Docking and Drug-Likeness Studies. *Mater. Today Proc.* **2021**, *45*, 7608–7614, https://doi.org/10.1016/j.matpr.2021.03.080.
34. Cramer, R. D.; Patterson, D. E.; Bunce, J. D. Comparative Molecular Field Analysis (CoMFA). 1. Effect of Shape on Binding of Steroids to Carrier Proteins. *J. Am. Chem. Soc.* **1988**, *110*, 5959–5967, https://doi.org/10.1021/ja00226a005.
35. Klebe, G.; Abraham, U.; Mietzner, T. Molecular Similarity Indices in a Comparative Analysis (CoMSIA) of Drug Molecules to Correlate and Predict Their Biological Activity. *J. Med. Chem.* **1994**, *37*, 4130–4146, https://doi.org/10.1021/jm00050a010.
36. Ståhle, L.; Wold, S. 6 Multivariate Data Analysis and Experimental Design in Biomedical Research. In *Progress in Medicinal Chemistry*; Elsevier, 1988; Vol. 25, pp 291–338, https://doi.org/10.1016/S0079-6468(08)70281-9.
37. El Khatabi, K.; Aanouz, I.; El-mernissi, R.; Khaldan, A.; Ajana, M.; Bouachrine, M.; Lakhlifi, T. *In silico* Analysis of 3D QSAR and Molecular Docking Studies to Discover New Thiadiazole-Thiazolone Derivatives as Mitotic Kinesin Eg5 Inhibition. *Moroc. J. Chem.* **2021**, *9*, 9–405, https://doi.org/10.48317/IMIST.PRSM/morjchem-v9i2.18721.
38. Golbraikh, A.; Tropsha, A. Beware of Q2! *J. Mol. Graph. Model.* **2002**, *20*, 269–276, https://doi.org/10.1016/S1093-3263(01)00123-1.
39. Tropsha, A.; Gramatica, P.; Gombar, V. The Importance of Being Earnest: Validation Is the Absolute Essential for Successful Application and Interpretation of QSPR Models. *QSAR Comb. Sci.* **2003**, *22*, 69–77, https://doi.org/10.1002/qsar.200390007.
40. Baroni, M.; Clementi, S.; Cruciani, G.; Costantino, G.; Riganelli, D.; Oberrauch, E. Predictive Ability of Regression Models. Part II: Selection of the Best Predictive PLS Model. *J. Chemom.* **1992**, *6*, 347–356, https://doi.org/10.1002/cem.1180060605.
41. Hajji, H.; En-nahli, F.; Aanouz, I.; Zaki, H.; Lakhlifi, T.; Ajana, M. A.; Bouachrine, M. Catastrophic Collision Between Obesity and COVID-19 Have Evoked the Computational Chemistry for Research *in silico* Design of New CaMKKII Inhibitors Against Obesity by Using 3D-QSAR, Molecular Docking, and ADMET. *Orbital Electron. J. Chem.* **2021**, *13*, 316–327, https://doi.org/10.17807/orbital.v13i4.1608.
42. Aanouz, I.; El Khatabi, K.; BelHassan, A.; Lakhlifi, T.; Elidrissi, M.; Bouachrine, M. 2D- and 3D-QSAR and Molecular Docking of 2-Hydroxyisoquinoline-1,3-Diones as Inhibitors of HIV Reverse Transcriptase. *Int. J. Quant. Struct.-Prop. Relatsh. IJQSPR* **2020**, *5*, 32–52, https://doi.org/10.4018/IJQSPR.2020100102.
43. Khaldan, A.; Bouamrane, S.; El-Mernissi, R.; El Khatabi, K.; Aanouz, I.; Aggoram, A.; Sbai, A.; Bouachrine, M.; Lakhlifi, T. QSAR Study of α-Glucosidase Inhibitors for Benzimidazole Bearing Bis-Schiff Bases Using CoMFA, CoMSIA, and Molecular Docking. *Int. J. Quant. Struct.-Prop. Relatsh. IJQSPR* **2021**, *6*, 9–24, https://doi.org/10.4018/IJQSPR.2021010102.
44. Aanouz, I.; Belhassan, A.; El Khatabi, K.; Lakhlifi, T.; El-Ldrissi, M.; Bouachrine, M. Moroccan Medicinal Plants as Inhibitors against SARS-CoV-2 Main Protease: Computational Investigations. *J. Biomol. Struct. Dyn.* **2021**, *39*, 2971–2979, https://doi.org/10.1080/07391102.2020.1758790.
45. DeLano, W. L. Pymol: An Open-Source Molecular Graphics Tool. *CCP4 Newsl. Protein Crystallogr.* **2002**, *40*, 82–92, http://148.79.162.84/newsletters/newsletter40/11_pymol.pdf.
46. Dassault Systèmes BIOVIA, Discovery Studio Modeling Environment, Release 2017. San Diego: Dassault Systèmes. (2016). Available online: https://www.3ds.com/products-services/biovia/products/molecular-modeling-simulation/biovia-discovery-studio/(accessed February 6, 2020).
47. Daina, A.; Michielin, O.; Zoete, V. SwissADME: A Free Web Tool to Evaluate Pharmacokinetics, Drug-Likeness and Medicinal Chemistry Friendliness of Small Molecules. *Sci. Rep.* **2017**, *7*, 42717, https://doi.org/10.1038/srep42717.
48. Pires, D. E. V.; Blundell, T. L.; Ascher, D. B. PkCSM: Predicting Small-Molecule Pharmacokinetic and Toxicity Properties Using Graph-Based Signatures. *J. Med. Chem.* **2015**, *58*, 4066–4072, https://doi.org/10.1021/acs.jmedchem.5b00104.

49. Gupta, S.; Singh, A. K.; Kushwaha, P. P.; Prajapati, K. S.; Shuaib, M.; Senapati, S.; Kumar, S. Identification of Potential Natural Inhibitors of SARS-CoV2 Main Protease by Molecular Docking and Simulation Studies. *J. Biomol. Struct. Dyn.* **2020**, *39*, 1–12, https://doi.org/10.1080/07391102.2020.1776157.
50. El Khatabi, K.; Aanouz, I.; El-Mernissi, R.; Singh, A. K.; Ajana, M. A.; Lakhlifi, T.; Kumar, S.; Bouachrine, M. Integrated 3D-QSAR, Molecular Docking, and Molecular Dynamics Simulation Studies on 1,2,3-Triazole Based Derivatives for Designing New Acetylcholinesterase Inhibitors. *Turk. J. Chem.* **2021**, *45*, 647–660, https://doi.org/10.3906/kim-2010-34.
51. Elhady, S. S.; Abdelhameed, R. F. A.; Malatani, R. T.; Alahdal, A. M.; Bogari, H. A.; Almalki, A. J.; Mohammad, K. A.; Ahmed, S. A.; Khedr, A. I. M.; Darwish, K. M. Molecular Docking and Dynamics Simulation Study of Hyrtios Erectus Isolated Scalarane Sesterterpenes as Potential SARS-CoV-2 Dual Target Inhibitors. *Biology* **2021**, *10*, 389, https://doi.org/10.3390/biology10050389.
52. Schmid, N.; Eichenberger, A. P.; Choutko, A.; Riniker, S.; Winger, M.; Mark, A. E.; van Gunsteren, W. F. Definition and Testing of the GROMOS Force-Field Versions 54A7 and 54B7. *Eur. Biophys. J.* **2011**, *40*, 843–856, https://doi.org/10.1007/s00249-011-0700-9.
53. Van Aalten, D. M. F.; Bywater, R.; Findlay, J. B. C.; Hendlich, M.; Hooft, R. W. W.; Vriend, G. PRODRG, a Program for Generating Molecular Topologies and Unique Molecular Descriptors from Coordinates of Small Molecules. *J. Comput. Aided Mol. Des.* **1996**, *10*, 255–262, https://doi.org/10.1007/BF00355047.
54. Parrinello, M.; Rahman, A. Polymorphic Transitions in Single Crystals: A New Molecular Dynamics Method. *J. Appl. Phys.* **1981**, *52*, 7182–7190, https://doi.org/10.1063/1.328693.
55. Hess, B.; Bekker, H.; Berendsen, H. J. C. LINCS: A Linear Constraint Solver for Molecular Simulations. *J. Comput. Chem.* **1997**, *18*, 1463–1472, https://doi.org/10.1002/(SICI)1096-987X(199709)18:12%3C1463::AID-JCC4%3E3.0.CO;2-H.
56. Darden, T.; York, D.; Pedersen, L. Particle Mesh Ewald: An $N \cdot \log(N)$ Method for Ewald Sums in Large Systems. *J. Chem. Phys.* **1993**, *98*, 10089–10092, https://doi.org/10.1063/1.464397.
57. Kushwaha, P. P.; Singh, A. K.; Bansal, T.; Yadav, A.; Prajapati, K. S.; Shuaib, M.; Kumar, S. Identification of Natural Inhibitors Against SARS-CoV-2 Drugable Targets Using Molecular Docking, Molecular Dynamics Simulation, and MM-PBSA Approach. *Front. Cell. Infect. Microbiol.* **2021**, *11*, 730288, https://doi.org/10.3389/fcimb.2021.730288.
58. Kushwaha, P. P.; Singh, A. K.; Prajapati, K. S.; Shuaib, M.; Gupta, S.; Kumar, S. Phytochemicals Present in Indian Ginseng Possess Potential to Inhibit SARS-CoV-2 Virulence: A Molecular Docking and MD Simulation Study. *Microb. Pathog.* **2021**, *157*, 104954, https://doi.org/10.1016/j.micpath.2021.104954.